Modelling Simul. Mater. Sci. Eng. **18** (2010) 055009 (17pp) doi:10.1088/0965-0393/18/5/055009

Structure, mechanical and thermodynamic stability of vacancy clusters in Cu

Qing Peng, Xu Zhang and Gang Lu

Department of Physics and Astronomy, California State University Northridge, Northridge, CA, USA

Received 5 January 2010, in final form 11 May 2010
Published 28 May 2010
Online at stacks.iop.org/MSMSE/18/055009

Abstract

The atomic structure, mechanical and thermodynamic stability of vacancy clusters in Cu are studied by atomistic simulations. The most stable atomic configuration of small vacancy clusters is determined. The mechanical stability of the vacancy clusters is examined by applying uniaxial and volumetric tensile strains to the system. The yield stress and yield strain of the system are significantly reduced compared with the perfect lattice. The dependence of vacancy formation and binding energy as a function of strain is explored and can be understood from the liquid-drop model. We find that the formation energy of the vacancy clusters decreases monotonically as a function of the uniaxial strain, while the formation energy increases first then decreases under the volumetric tensile strain. The thermodynamic stability of the vacancy clusters is analyzed by calculating the Helmholtz free binding energy and the total probability of dissociation of the vacancy clusters at 300 and 900 K under uniaxial and volumetric strains. We find that although most of the vacancy clusters appear to be thermodynamically stable, some of the intermediate sized clusters have a high probability of dissociation into smaller clusters.

(Some figures in this article are in colour only in the electronic version)

1. Introduction

Vacancies are the predominant point defects in metals and they could have a profound influence on materials' properties, ranging from mechanical strength [1–3], deformation behavior [4, 5], kinetic transport and diffusion [6, 7], to electrical conductivity and heat capacity [8, 9], to name a few. Thus the study of vacancy effects on the properties of technologically important materials, such as Cu, is of considerable interest. For all these properties, stress plays crucial roles. For example, it is generally believed that hydrostatic tensile stress is the driving force for the stress-void nucleation [10] and stress gradients are responsible for the void growth [11]. This work touches upon the stress induced voiding, which is one of the most important factors that causes failures of the ultra-large integrated circuits with Cu-based interconnects [12]. In

this case, the stress is built up as a result of the mismatch in thermal expansion coefficients between the metal lines and the surrounding dielectrics [13]. There are other interesting problems related to the void growth and coalescence under various loading conditions [14–19]. For example, TEM observations have been performed for neutron-irradiated Cu at 300 °C which verify the transition from stacking fault tetrahedra (SFT) to voids, depending on the size of the vacancy cluster. These observations are consistent with the embedded-atom-method (EAM) simulations [20]. A direct transition from a 20-vacancy cluster to an SFT was also found by using parallel replica EAM molecular dynamics simulations [16]. We have recently studied void formation by using the multiscale method and discovered a connection between vacancy-induced bonding cages and the tendency for void formation in fcc metals [22].

In this paper, we use atomistic simulations based on the EAM potential to (1) determine the structure of the most stable n-vacancy clusters where $n \leqslant 21$; (2) examine the mechanical stability of Cu containing vacancy clusters; (3) study the dependence of the vacancy cluster formation energy and binding energy as a function of the uniaxial and volumetric tensile stress; (4) examine the thermal stability of the vacancy clusters at different temperatures. The computational method is given in section 2. The convergence of the vacancy formation energy is studied in section 3.1; the structure of the vacancy clusters is determined in section 3.2 and the mechanical stability of the vacancy clusters is examined in section 3.3 for both the uniaxial and volumetric tensile strains. Finally the thermal stability of the vacancy clusters is considered in section 3.4 and the conclusion is in section 4.

2. The computational method

A cubic supercell with the periodic boundary conditions along three directions is used in the simulations. The supercell is oriented in the cubic directions, i.e. x in [1 0 0], y in [0 1 0] and z in [0 0 1], respectively. The atomic interaction of Cu is described by an EAM potential [23]. The atomic relaxation is carried out with molecular statics implemented in the LAMMPS codes [24]. It is well established that the EAM potential is capable of providing reasonable atomic structure and energetics for vacancies in Cu [14, 16, 17, 20, 21].

The vacancy cluster formation energy, which describes the energy cost for forming a vacancy cluster with respect to the perfect lattice, is computed for various vacancy clusters, in the presence or absence of external strains. Specifically, under a strain ϵ the vacancy cluster formation energy, $E^{\mathrm{F}}_{n\mathrm{v},\epsilon}$, of a given n-vacancy cluster in an N-atom supercell is defined as

$$E^{\mathrm{F}}_{n\mathrm{v},\epsilon} = E^{\mathrm{tot}}_{n\mathrm{v},\epsilon}(N-n) - \frac{N-n}{N} E^{\mathrm{tot}}_{0,\epsilon}(N), \tag{1}$$

where $E^{\mathrm{tot}}_{n\mathrm{v},\epsilon}(N-n)$ is the total energy of the supercell containing $(N-n)$ atoms with an n-vacancy cluster under strain ϵ and $E^{\mathrm{tot}}_{0,\epsilon}(N)$ is the total energy of the supercell containing N atoms in a perfect lattice with a strain of ϵ. It is convenient to use the formation energy per vacancy $E^{\mathrm{f}}_{n\mathrm{v},\epsilon}$ to compare among different vacancy clusters, which is defined as

$$E^{\mathrm{f}}_{n\mathrm{v},\epsilon} = E^{\mathrm{F}}_{n\mathrm{v},\epsilon}/n. \tag{2}$$

Another important quantity calculated is the vacancy binding energy, $E^{\mathrm{B}}_{n\mathrm{v},\epsilon}$, which describes the energy gain when n monovacancies are combined into an n-vacancy cluster. The binding energy of an n-vacancy cluster under a strain ϵ is given by

$$E^{\mathrm{B}}_{n\mathrm{v},\epsilon} = nE^{\mathrm{f}}_{1\mathrm{v},\epsilon} - E^{\mathrm{F}}_{n\mathrm{v},\epsilon}. \tag{3}$$

A positive value of $E^{\mathrm{B}}_{n\mathrm{v},\epsilon}$ suggests that it is energetically favorable for the n monovacancies to form an n-vacancy cluster at zero temperature under the strain. Similarly, one can define

the binding energy per vacancy, $E^{\mathrm{b}}_{n\mathrm{v},\epsilon}$, to facilitate the comparison among different vacancy clusters, which is given by

$$E^{\mathrm{b}}_{n\mathrm{v},\epsilon} = E^{\mathrm{B}}_{n\mathrm{v},\epsilon}/n = E^{\mathrm{f}}_{1\mathrm{v},\epsilon} - E^{\mathrm{f}}_{n\mathrm{v},\epsilon}. \tag{4}$$

In order to determine the thermodynamic stability of a vacancy cluster, we need to calculate the dynamical matrix and the Helmholtz free energy of the defect system. Under the harmonic approximation, the dynamical matrix under a strain ϵ is defined as follows:

$$D^{\alpha,\beta}_{i,j} = \frac{1}{m}\frac{\partial^2 E^{\mathrm{tot}}_{\epsilon}}{\partial u^{\alpha}_i \partial u^{\beta}_j}, \tag{5}$$

where m is the mass of the atoms, u^{α}_i and u^{β}_j are the displacement of atom i and j in direction α and β, respectively, from its relaxed equilibrium position. $E^{\mathrm{tot}}_{\epsilon}$ is the total energy of the system. The vacancy formation entropy is evaluated via the equation [25, 26]

$$S^{\mathrm{F}}_{n\mathrm{v},\epsilon} = -k_{\mathrm{B}}\left(\sum_{i=1}^{3(N-n-1)} \ln \omega^{n\mathrm{v},\epsilon}_i - \frac{N-n-1}{N-1}\sum_{i=1}^{3(N-1)} \ln \omega^{0,\epsilon}_i\right), \tag{6}$$

where $\omega^{n\mathrm{v},\epsilon}_i$ and $\omega^{0,\epsilon}_i$ represent the harmonic vibrational frequency for the system with and without vacancies, respectively. Three acoustic phonon frequencies are removed from the sum owing to the translational invariance of the system. Analogous to the definition of the binding energy, the binding entropy is defined as

$$S^{\mathrm{B}}_{n\mathrm{v},\epsilon} = nS^{\mathrm{F}}_{1\mathrm{v},\epsilon} - S^{\mathrm{F}}_{n\mathrm{v},\epsilon}, \tag{7}$$

where $S^{\mathrm{F}}_{1\mathrm{v},\epsilon}$ and $S^{\mathrm{F}}_{n\mathrm{v},\epsilon}$ are the formation entropy of a monovacancy and an n-vacancy cluster, respectively.

To compute the dynamical matrix, we choose a block consisting of 4000 atoms with the vacancy cluster placed in the center. The dynamical matrix is determined by displacing the atoms ± 0.01 Å from their relaxed equilibrium positions in all three Cartesian directions [26]. The dynamical matrix with the dimensions 12 000 $\times$ 12 000 is then diagonalized and the eigen-frequencies are obtained to evaluate the formation entropy. The Helmholtz binding free energy of an n-vacancy cluster at temperature T is determined as

$$A^{\mathrm{B}}_{n\mathrm{v},\epsilon} = E^{\mathrm{B}}_{n\mathrm{v},\epsilon} - TS^{\mathrm{B}}_{n\mathrm{v},\epsilon}, \tag{8}$$

The positive (negative) value of $A^{\mathrm{B}}_{n\mathrm{v},\epsilon}$ indicates the n-vacancy cluster is thermodynamically stable (unstable) against a simultaneous dissociation into n monovacancies.

3. Results and analysis

3.1. Convergence of vacancy formation energy

A convergence test is carried out to determine the sufficient system size (in the unit of a_0, where $a_0 = 3.615$ Å), and the results are shown in figure 1. For a monovacancy, we find that $6a_0$ is enough to reach convergence for the vacancy formation energy, while for a 21-vacancy cluster (the largest vacancy cluster in this study), $20a_0$ appears to be sufficient. Therefore, in all our calculations, we use $20a_0$ as the system size. With a supercell of $20a_0 \times 20a_0 \times 20a_0$ (32 000 lattice sites), we found that the monovacancy formation energy is 1.2837 eV, which agrees very well with previous calculations [27, 28].

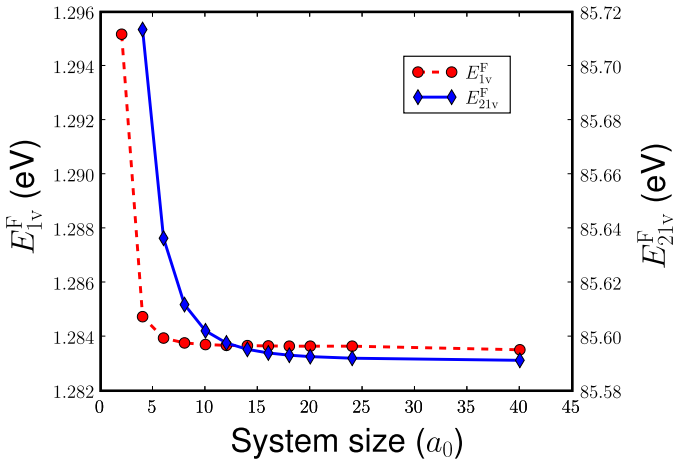

Figure 1. The convergence test of the vacancy formation energy (in eV) with respect to the system size (unit of a_0) for a monovacancy (dashed line, scaled to the left axis) and a 21-vacancy cluster (solid line, scaled to the right axis).

3.2. Atomic structure of n-vacancy clusters

Vacancy clusters containing up to 21 vacancies are studied in this work. For each n-vacancy cluster, several most stable configurations are considered, especially in planar, tetrahedral and spherical structures. These structures are emphasized owing to their relevance to vacancy loops, SFT and spherical voids, observed in experiments [2]. For each n, the structure with the maximum binding energy is regarded as the most energetically stable configuration for the n-vacancy cluster.

The most stable di-vacancy is the one where two vacancies are the nearest neighbors. The binding energy is 0.158 eV, agreeing well with the previous calculations [27, 28]. Starting from the most stable di-vacancy, we can search for the most stable tri-vacancy by placing the third vacancy at various nearest-neighbor positions. The configuration of the highest binding energy of a tri-vacancy is shown in figure 2(*a*) and $E^{\mathrm{B}}_{3v} = 0.474$ eV. The three vacancies form an equilateral triangle lying on the $\{1\,1\,1\}$ plane, and are mutually nearest-neighbors. Starting from the most stable tri-vacancy, we considered six most probable configurations for a four-vacancy cluster, and found that the equilateral tetrahedron formed by four nearest-neighbor vacancies has the highest binding energy of $E^{\mathrm{B}}_{4v} = 0.94$ eV. The atomic structure of the tetra-vacancy is shown in figure 2(*b*).

In the same manner, we explored the most stable atomic configurations for all vacancy clusters with $n \leqslant 21$. For example, we found that the most stable 5-vacancy cluster (penta-vacancy) is a squared pyramid with a binding energy of $E^{\mathrm{B}}_{5v} = 1.372$ eV, shown in figure 2(*c*). The most stable 6-vacancy cluster (hexa-vacancy) is an octahedron shown in figure 2(*d*) with a binding energy of $E^{\mathrm{B}}_{6v} = 2.113$ eV. Interestingly, we found that the most stable configuration of a 10-vacancy cluster is not an equilateral tetrahedron shown in figure 2(*e*), but rather a less symmetric structure shown in figure 2(*f*). For $n = 13$, the most stable structure resembles a sphere, with one vacancy at the center, and 12 nearest neighbors surrounding it. The radius of the sphere is $\sqrt{2}/2a_0$ shown in figure 2(*g*). For $n > 13$, the vacancy clusters tend to form three-dimensional voids, appearing more like spheres than tetrahedra. For example, the structure of a 19-vacancy cluster is shown in figure 2(*h*); it has one vacancy at the center, and 12 nearest

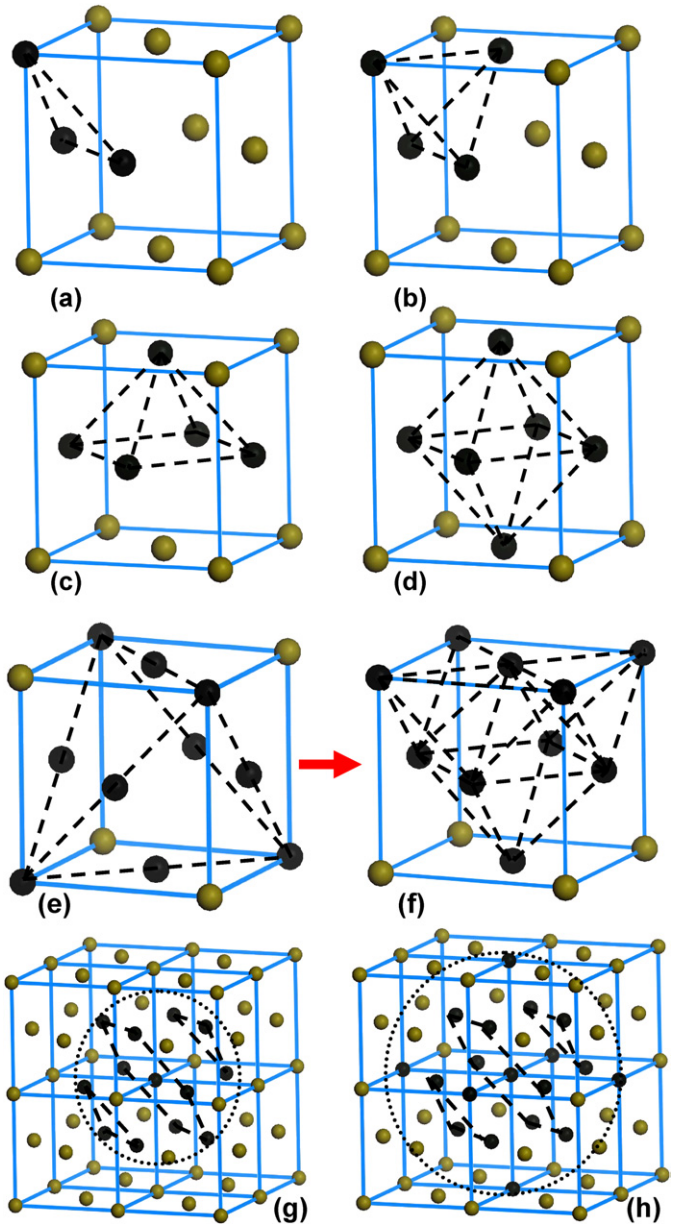

Figure 2. The most stable atomic configurations for 3, 4, 5, 6, 10, 13 and 19-vacancy clusters. The black and gray spheres represent the vacancy and atom, respectively. Note that the most stable configuration for the 10-vacancy cluster is not the symmetrical one shown in (*e*), but rather the one with less symmetry shown in (*f*).

neighbors and 6 second-nearest neighbors of the central vacancy filling the sphere of a radius of a_0.

The formation energy per vacancy $E^f_{n\mathrm{V}}$ (in eV) for all vacancy clusters is presented in figure 3. Overall, the formation energy decreases with respect to the cluster size, which can be understood from the liquid-drop model for metals [29, 30]. In this model, the void formation

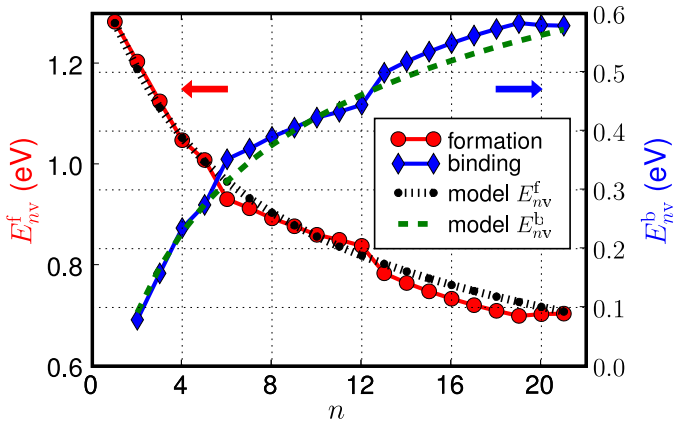

Figure 3. The formation energy (circle, scaled to left, in eV) and binding energy (diamond, scaled to right, in eV) per vacancy of the n-vacancy clusters. The dotted–dashed line and dashed line are the prediction of $E^{\rm f}_{n\rm v}$ and $E^{\rm b}_{n\rm v}$ from the liquid-drop model, respectively.

energy can be approximated as

$$E^{\rm F}_{\rm void} = 4\pi R^2_{\rm WS}\sigma - 2\pi R_{\rm WS}\gamma, \tag{9}$$

where $R_{\rm WS} = (3V/4\pi)^{1/3}$ is the Wigner–Seitz radius of the void with volume V; σ is the surface energy density and γ is the curvature energy [29]. The volume of an n-vacancy cluster can be approximated as $V_n \approx n v_0$, where v_0 is the volume of a monovacancy. Therefore equation (9) can be rewritten as

$$E^{\rm f}_{n\rm v} = c_1 n^{-\frac{1}{3}} - c_2 n^{-\frac{2}{3}}, \tag{10}$$

where $c_1 = 4\pi\sigma(3v_0/4\pi)^{2/3}$ and $c_2 = 2\pi\gamma(3v_0/4\pi)^{1/3}$. Taking $\sigma = 0.0932\,\text{eV Å}^{-2}$, $\gamma = 0.119\,\text{eV Å}^{-1}$ and $v_0 = a_0^3/4$, equation (10) is plotted in figure 3, which matches very well the atomistic results. The value of σ and γ is taken from [29]. σ is close to the EAM surface energy density of Cu: $0.08\,\text{eV Å}^{-2}$ for the (1 1 0) surface and $0.114\,\text{eV Å}^{-2}$ for the (1 1 1) surface. Interestingly, we find that the formation energy curve becomes flatter as n becomes larger, and approaches an asymptotic value of 0.7 eV. This value is very close to the monovacancy formation energy on a flat (1 1 1) surface of Cu, which is 0.73 eV. The reason for this asymptotic behavior is that as the vacancy cluster becomes larger, the curvature of the void surface becomes smaller, and thus the formation energy approaches the value of a monovacancy on a flat surface. It should be noted that although equation (9) neglects the elastic energy associated with the strain field existing around a vacancy cluster, it nonetheless captures the essential physics, i.e. the void formation depends on the competition of the surface energy and the curvature energy, that underlies the overall dependence of the formation energy as a function of the cluster size.

We also present the binding energy per vacancy (in eV) as a function of n in figure 3, shown in the diamond curve and scaled to the right axis. The binding energy increases monotonically with n, and is positive for all vacancy clusters, suggesting that the monovacancies prefer to aggregate in Cu, in order to reduce the number of broken bonds. From equations (10) and (4), we can express $E^{\rm b}_{n\rm v}$ as

$$E^{\rm b}_{n\rm v} = c_1(1 - n^{-\frac{1}{3}}) - c_2(1 - n^{-\frac{2}{3}}), \tag{11}$$

which is plotted as the dashed line in figure 3. It appears that the liquid-drop model reproduces the atomistic results surprisingly well.

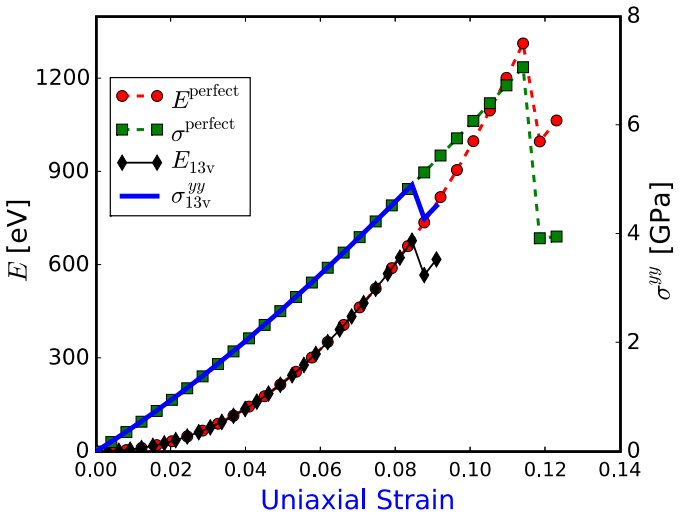

Figure 4. The strain energy (scale to the left axis, in eV) and stress (scale to the right axis, in GPa) veersus uniaxial tensile strain for a 13-vacancy cluster (diamond and solid line) and perfect lattice (circle and square), respectively.

3.3. Mechanical stability

In this section, we examine the mechanical stability of the vacancy clusters by applying external uniaxial tensile strains and volumetric tensile strains to the system. The tensile strains as opposed to compression strains are considered because the former often appear in Cu interconnects as a result of thermal expansions. The strain-free structures of the vacancy clusters are taken from the results obtained in section 3.2.

3.3.1. Uniaxial tensile strain. The uniaxial tensile strain is applied along the y axis, and the x and z axes are free to change by conserving the volume. The strain is applied quasi-statically, with each loading that is 1.001 times that of the previous step. We examine the mechanical response of the vacancy clusters by showing the strain energy and the tensile stress σ_{yy} as a function of the applied strain ϵ_{yy}. Because the results of all vacancy clusters follow the same pattern, we select the 13-vacancy cluster as a representative to illustrate the salient features of the results. As shown in figure 4, we find that both the strain energy and the tensile stress increase monotonically with the strain initially, followed by a sudden drop at the yield point. The system behaves in a linear elastic fashion, i.e. the energy increases quadratically and the stress increases linearly. There are two importance results: (1) the perfect and the defect lattice have almost identical elastic behavior—the two curves coincide with each other for both the energy and the stress. (2) The presence of the vacancy defect significantly reduces the yield strength of the material. The yield stress and strain are 7.32 GPa and 0.117 for the perfect lattice and 4.98 GPa and 0.085 for the defect system, respectively. At the yield point (the drop in the curves), dislocations are nucleated and propagate through the system, as shown by the central symmetry parameter (CSP) [4, 31] plot in figure 5. CSP is defined as $\mathrm{CSP} = \sum_{i=1}^{6} |R_i + R_{i+6}|^2/24D^2$, where R_i and R_{i+6} are the vectors or bonds corresponding to the six pairs of opposite nearest neighbors in the deformed fcc lattice [31] and D is the nearest-neighbor distance in the perfect fcc lattice. For each atom, there is a CSP value associated with it. Dislocation cores and stacking faults correspond to the CSP values ranging between 0.003

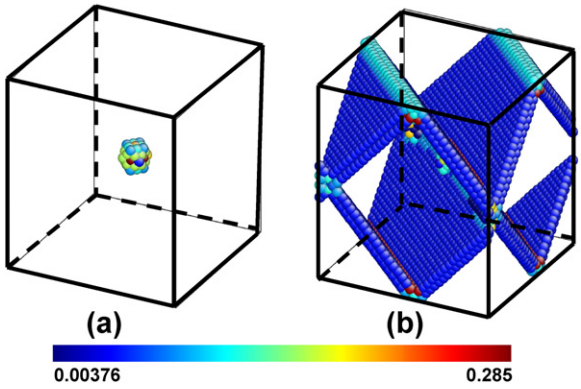

Figure 5. CSP plot for the system immediately before (*a*) and after (*b*) the yield point. The color bar represents the magnitude of the CSP values in the system.

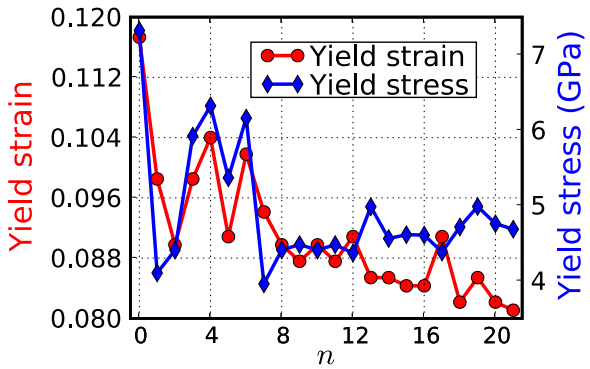

Figure 6. The yield strain (circle, scaled to the left) and yield stress (diamond, scaled to the right, in GPa) of the n-vacancy clusters under the uniaxial strain.

and 0.1. Just before the yielding, there is no dislocation in the system (figure 5(*a*)) while just after the yielding, dislocations appear (figure 5(*b*)).

In figure 6, we present the yield strain (left axis) and yield stress (right axis, in GPa) as a function of n. Overall, the yield strain follows approximately the yield stress, and for large vacancy clusters, the yield stress/strain is significantly reduced compared with the perfect lattice.

We have calculated the formation energy $E^{\mathrm{f}}_{nv,\epsilon}$ (in eV) of the vacancy clusters under the uniaxial strain up to 0.062 beyond which some of the defect systems start yielding. The results are summarized in figure 7 for representative vacancy clusters—the results of all vacancy clusters have the same general features. It is found that the formation energy decreases monotonically as a function of strain for all clusters. This is because the vacancy formation energy results from the energy cost of bond breaking around the vacancies. By applying the tensile stress, the bonds are weakened owning to the stretching, therefore it would cost less energy to break them compared with the strain-free case. The present result is consistent with that in Al obtained by orbital-free density functional theory calculations [32]. It appears that some of the energy curves tend to converge (or cross) at larger strains, for example, $n = 5, 6, 10$. The apparent convergence suggests that a large stress can change the relative

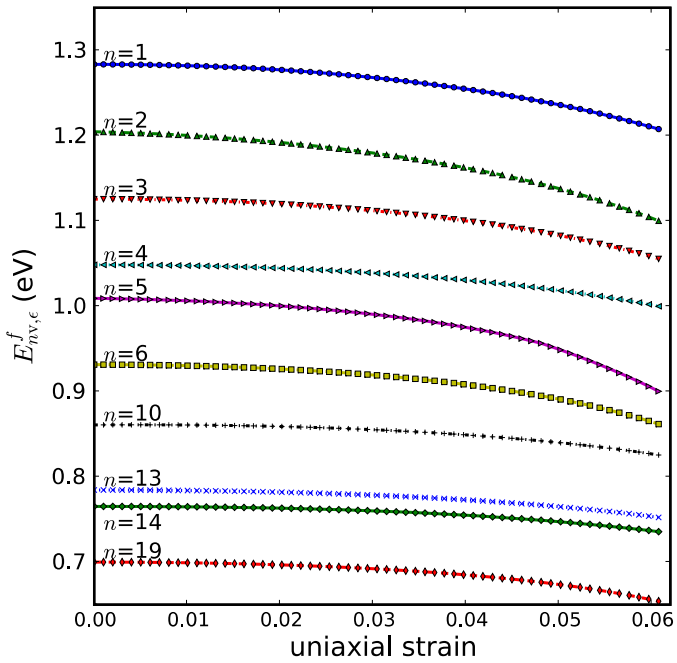

Figure 7. The formation energy per vacancy $E^{\mathrm{f}}_{n\mathrm{v},\epsilon}$ (in eV) under the uniaxial strain ϵ for several representative vacancy clusters.

stability of vacancy clusters of different sizes, which may trigger structural changes among them.

To examine how mechanical stability depends on the orientation of the applied strain, we carried out additional calculations for a di-vacancy under uniaxial strains. The di-vacancy is placed along the $[\bar{1}\,1\,0]$ direction. The supercell consists of $51 \times 51 \times 51$ Å^3 which contains 11 200 atoms. The strain is applied to the system along $[1\,1\,0]$, $[\bar{1}\,1\,0]$, $[0\,0\,1]$ and a tilted direction, $[0\,1\,0]$, respectively. The result of the formation energy $E^f_{2\mathrm{v},\epsilon}$ is plotted in figure 8. The general trend that the vacancy formation energy decreases with the applied strain is still valid, consistent with the previous results of other n-vacancy clusters. The result also indicates that the mechanical behavior is orientation-dependent on the strain. For example, for the strain along $[0\,0\,1]$, the vacancy formation energy would increase first and then decrease. Because of the complexity of the energetics as a function of strain directions, in the following we will only focus on two simplest cases, the uniaxial and volumetric strain for larger vacancy clusters.

The binding energy per vacancy $E^{\mathrm{b}}_{n\mathrm{v},\epsilon}$ (in eV) is shown in figure 9. The binding energy remains positive for all strains less than 0.062. For most of the vacancy clusters, the binding energy decreases as a function of the strain because the attractive vacancies are pulled apart by the stress. It appears that large strains could lead to break-up or re-arrangement of the vacancy clusters.

3.3.2. Isotropic volumetric tensile strain. Next we study the behavior of the vacancy clusters under isotropic volumetric tensile deformations. In this case of triaxial loading, the volume of the system is no longer conserved, but with an equal strain applied along the x,y,z directions

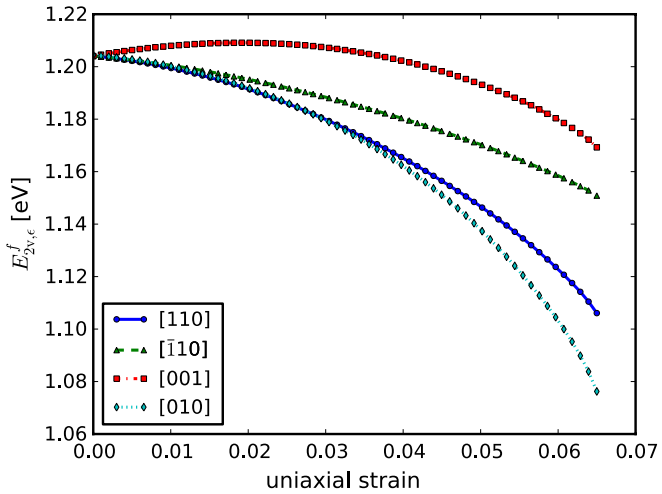

Figure 8. The formation energy per vacancy $E^{\mathrm{f}}_{2\mathrm{v},\epsilon}$ (in eV) as a function of the uniaxial strain in different directions.

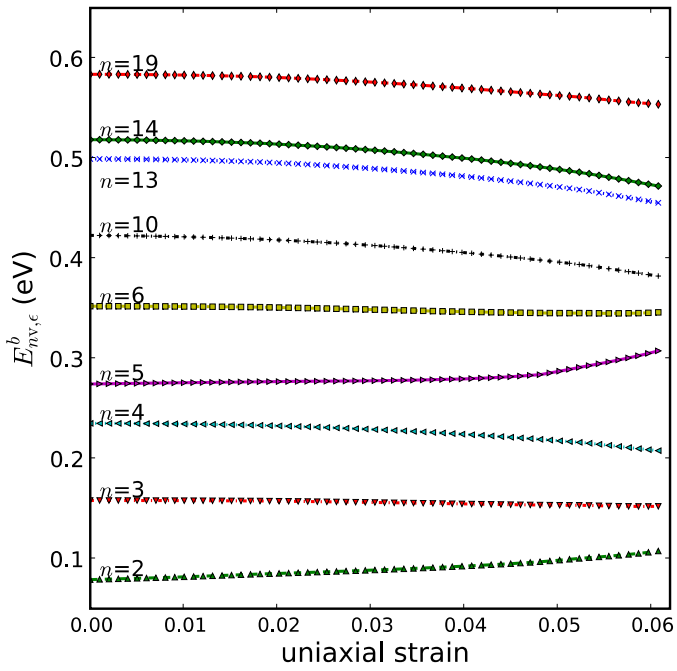

Figure 9. The binding energy per vacancy $E^{\mathrm{b}}_{n\mathrm{v},\epsilon}$ (eV) under the uniaxial strain ϵ for several representative vacancy clusters.

simultaneously. At each deformation step, the size of the simulation box is 1.0005 times that of the previous step.

The strain energy and stress as a function of the strain are shown in figure 10, with $n = 13$ as a representative because all vacancy clusters behave in the same way. The energy increases with the strain before the drop at a volume strain of $\epsilon = 0.13$. The drop of the energy is an indication

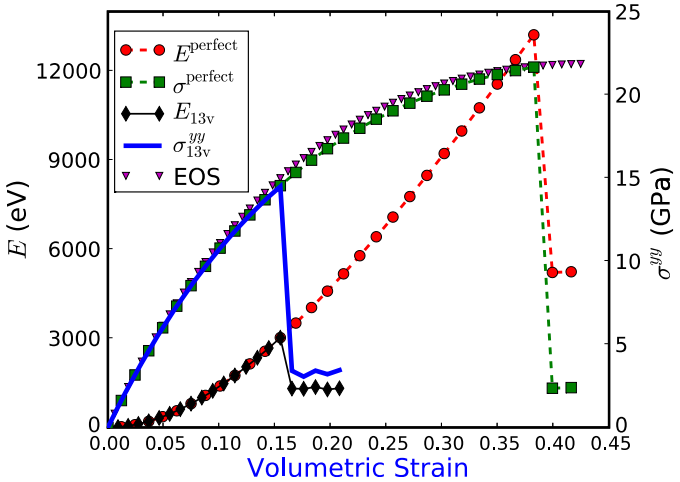

Figure 10. The strain energy (scale to the left axis, in eV) and stress (scale to the right axis, in GPa) versus isotropic volumetric strain for a 13-vacancy cluster (diamond and solid line) and the perfect lattice (circle and square), respectively. The triangle curve represents the EOS from equation (13).

of the onset of plasticity of the system. The stress drops at the same strain as the energy. The CSP plot (not shown here) indicates that dislocations are nucleated all over the system. At this point, we have to terminate the calculations because the close proximity between the dislocation loops across the computational cell will render the simulations worthless. For the isotropic volumetric tensile strain, $\sigma^{yy} = \sigma^{xx} = \sigma^{xx} = -P$, and P is the pressure. The non-linear behavior of the stress–strain relation in figure 10 can be understood from the equation of state (EOS) of solids [33]:

$$P(V) = \frac{3K_0(1-x)}{x^2} \exp[\xi(1-x)], \tag{12}$$

where V_0 and K_0 are the volume and the bulk modulus of the solid at equilibrium; $x \equiv (V/V_0)^{1/3}$, $\xi \equiv \frac{3}{2}(K_0' - 1)$ and $K_0' \equiv \partial K_0/\partial P|_{P=0}$. For the volumetric loading, $V = V_0(1+\epsilon)$ and $x - 1 \approx \frac{1}{3}\epsilon$, thus we can rewrite equation (12) as

$$\sigma(\epsilon) = \frac{K_0\epsilon}{(1+\epsilon/3)^2} \exp\left[-\frac{\xi\epsilon}{3}\right]. \tag{13}$$

Equation (13) is plotted as the triangle curve in figure 10 and it agrees very well with the EAM result by taking the experimental value of $K_0 = 140$ GPa and $\xi = 5.2$.

The yield strain and yield stress for all vacancy clusters under the volumetric deformation are plotted in figure 11. The energy/stress curves of the defect systems trace closely to that of the perfect lattice, indicating that the vacancy clusters do not change the behavior of the material before yielding. Overall, both the yield stress and strain decrease as a function of n, suggesting that vacancy clusters can drastically reduce the yield strength of the material. It should be noted that the quantitative values of the yield stress/strain obtained here do not correspond to the realistic situation due to the high vacancy concentrations in the simulations; however, the qualitative features remain valid.

The formation energy per vacancy (in eV) under the volumetric tensile strain is shown in figure 12. Overall, we find that the formation energy first increases with the strain to a maximum and then decreases; this is different from the uniaxial case. The difference is due

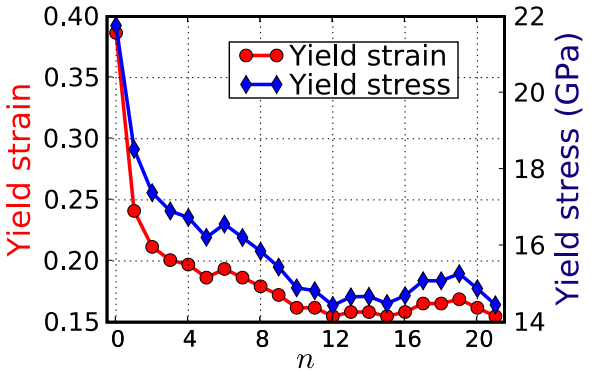

Figure 11. The yield strain (circle, scaled to the left) and stress (cross, scaled to the right, in GPa) of the n-vacancy clusters under the volumetric tensile strain.

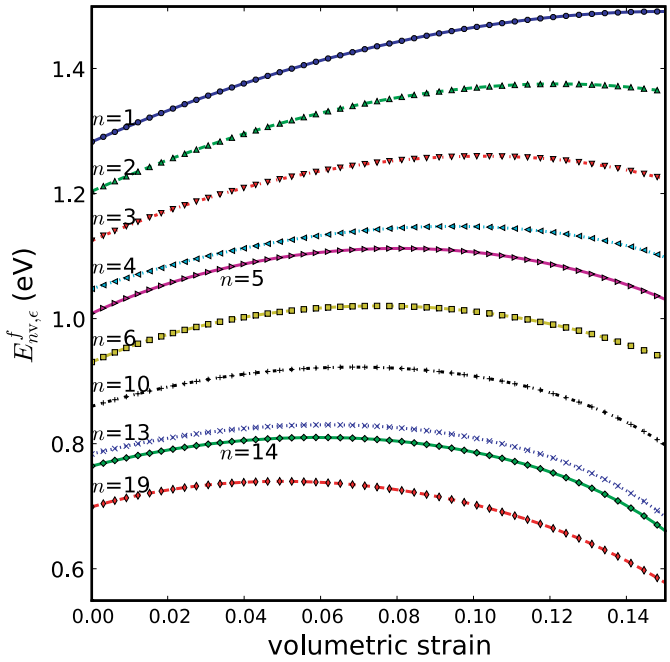

Figure 12. The formation energy per vacancy $E^{\mathrm{f}}_{nV,\epsilon}$ (in eV) under the volumetric strain ϵ for several representative vacancy clusters.

to the different loading conditions: in the uniaxial case, the volume of the system is fixed, therefore to a good approximation, the surface area of the void is also fixed. On the other hand, the surface area of the void increases as the volume increases in the triaxial case, therefore the inner surface energy increases as a function of the tensile strain. The increasing surface energy dominates the decreasing bonding energy contribution at small strains, hence the formation energy reaches a maximum at an immediate strain. For small vacancy clusters, such as $n = 1$ and $n = 2$, the surface energy contribution is negligible owing to the small size of the vacancy clusters, thus their formation energy increases monotonically.

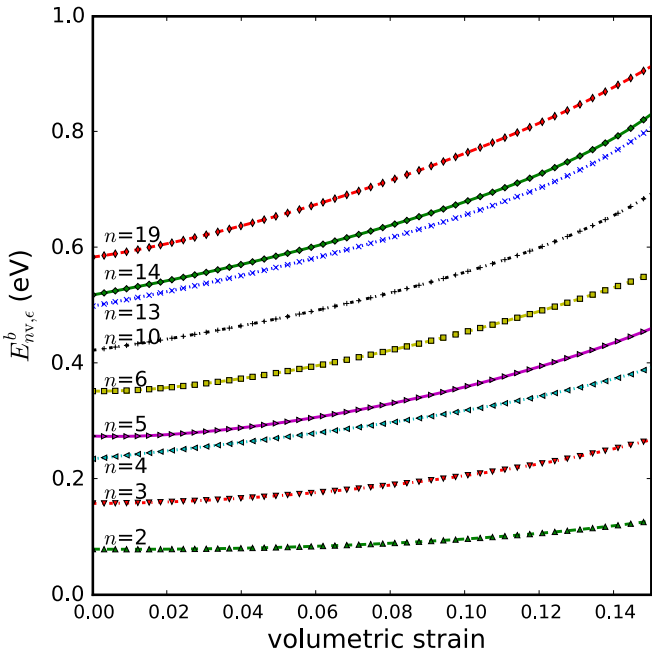

Figure 13. The binding energy per vacancy $E^{\mathrm{b}}_{nv,\epsilon}$ (in eV) under the volumetric strain ϵ for several representative vacancy clusters.

For the volumetric strain, the binding energy per vacancy increases monotonically with the strain, and it increases faster when n is larger (figure 13). Such a behavior can be understood again from the liquid-drop model. Under the volumetric strain ϵ, the volume of a monovacancy is $v_0(1+\epsilon_{11})^3$ where the linear strain $\epsilon_{11} \approx \epsilon/3$. Thus the two coefficients in equation (11) become $c_1(1+\epsilon_{11})^2$ and $c_2(1+\epsilon_{11})$, respectively. $E^{\mathrm{b}}_{nv,\epsilon}$ can then be expressed as a quadratic function of ϵ_{11} or ϵ:

$$E^{\mathrm{b}}_{nv,\epsilon} = c_1(1-n^{-\frac{1}{3}})(1+\epsilon_{11})^2 - c_2(1-n^{-\frac{2}{3}})(1+\epsilon_{11}) = c_1(1-n^{-\frac{1}{3}})\epsilon_{11}^2 + [2c_1(1-n^{-\frac{1}{3}}) - c_2(1-n^{-\frac{2}{3}})]\epsilon_{11} + c_1(1-n^{-\frac{1}{3}}) - c_2(1-n^{-\frac{2}{3}}). \quad (14)$$

Since $c_1(1-n^{-\frac{1}{3}}) > 0$ and $[2c_1(1-n^{-\frac{1}{3}}) - c_2(1-n^{-\frac{2}{3}})] > 0$, $E^{\mathrm{b}}_{nv,\epsilon}$ would increase monotonically with the volumetric strain ϵ. The larger the n value, the larger the coefficient of the quadratic term $c_1(1-n^{-\frac{1}{3}})$, hence $E^{\mathrm{b}}_{nv,\epsilon}$ increases faster with respect to the strain.

3.4. Thermodynamic stability

In previous sections, the analysis is based on the energy at zero temperature. However, larger vacancy clusters (or even voids) are formed in a non-equilibrium supersaturated vacancy atmosphere at finite temperatures. In order to employ the well-established classical nucleation theory [35–37] which can give a precise thermodynamic description of void formation, we need to obtain Helmholtz free energies for the vacancy clusters. It is important to point out that the entropy term in the Helmholtz free energy has two contributions. One is the configurational entropy (or entropy of mixing) which takes into account the probabilities of n vacancies occupying N_{latt} lattice sites, resulting in the familiar expression of vacancy concentration in

equation (15). The other one is the vibrational entropy of the vacancy clusters shown in equation (6). In thermal equilibrium, the concentration of an n-vacancy cluster is given by

$$c_{n\mathrm{v}} = \frac{g_{n\mathrm{v}}}{n} \mathrm{e}^{-A^{\mathrm{F}}_{n\mathrm{v},\epsilon}/k_{\mathrm{B}}T}, \tag{15}$$

where $g_{n\mathrm{v}}$ is the coordination number of the n-vacancy cluster [34]; it is equal to the number of possible atomic configurations of an n-vacancy cluster, e.g. $g_{2\mathrm{v}} = 6$ for a di-vacancy and $g_{3\mathrm{v}} = 8$ for a tri-vacancy. The Helmholtz formation free energy $A^{\mathrm{F}}_{n\mathrm{v},\epsilon}$ consists of the formation energy $E^{\mathrm{F}}_{n\mathrm{v},\epsilon}$ in equation (1) and the formation entropy $S^{\mathrm{F}}_{n\mathrm{v},\epsilon}$ in equation (6).

In the following, we will address the thermodynamic stability of the vacancy clusters. At finite temperatures T, a vacancy cluster could dissociate into smaller clusters or eventually into monovacancies. As there are many different ways that a larger vacancy cluster can thermally dissociate into smaller ones, we use the concept of total probability to dissociation $P_{\mathrm{tot}}(n)$ [22] to analyze the thermal stability of the vacancy clusters. Here we cite the formulae that were used to calculate $P_{\mathrm{tot}}(n)$ in [22]. The equations are reproduced in the following. $P_{\mathrm{tot}}(n)$ can be expressed as $P_{\mathrm{tot}} = \sum_i P_i(n)$ where $P_i(n)$ represents the probability of a particular—say, the ith way—dissociation. For example, an n-vacancy cluster may dissociate into n monovacancies simultaneously, whose probability $P_1(n)$ is given by

$$P_1(n) = \frac{(c_{1\mathrm{v}})^n}{c_{n\mathrm{v}}} = \frac{n}{g_{n\mathrm{v}}} \mathrm{e}^{-(nA^{\mathrm{F}}_{1\mathrm{v},\epsilon} - A^{\mathrm{F}}_{n\mathrm{v},\epsilon})/k_{\mathrm{B}}T} \tag{16}$$

$$= \frac{n}{g_{n\mathrm{v}}} \mathrm{e}^{-A^{\mathrm{B}}_{n\mathrm{v},\epsilon}/k_{\mathrm{B}}T}; \tag{17}$$

or an n-vacancy cluster could break into a monovacancy plus an $(n-1)$-vacancy cluster, whose probability $P_2(n)$ is expressed as

$$P_2(n) = \frac{c_{1\mathrm{v}} c_{(n-1)\mathrm{v}}}{c_{n\mathrm{v}}} \tag{18}$$

$$= \frac{n g_{(n-1)\mathrm{v}}}{(n-1) g_{n\mathrm{v}}} \mathrm{e}^{-(A^{\mathrm{B}}_{n\mathrm{v},\epsilon} - A^{\mathrm{B}}_{(n-1)\mathrm{v},\epsilon})/k_{\mathrm{B}}T}. \tag{19}$$

To be more specific, let us consider the probability $P_{\mathrm{tot}}(4)$: we need to evaluate $P_1(4)$, $P_2(4)$, $P_3(4)$ and $P_4(4)$, and they represent the probabilities of dissociating a 4-vacancy cluster into four monovacancies ($4 = 1+1+1+1$), a monovacancy and a tri-vacancy cluster ($4 = 1+3$), two di-vacancies ($4 = 2+2$) and two monovacancies and a di-vacancy ($4 = 1+1+2$), respectively. In principle, we should consider all possible combinations in calculating a given $P_{\mathrm{tot}}(n)$. However, because for larger vacancy clusters such as $n > 8$, there are too many possible dissociation paths and most of them have vanishing probability, we only consider the contributions of the dominating dissociation paths. On the other hand, for smaller clusters with $n \leqslant 8$, we consider all possible dissociation paths. Since the concentration $c_{n\mathrm{v}}$ represents the probability of an n-vacancy cluster in a lattice, the ratio of the relevant concentrations in equations (16)–(17) indicates the probability of a larger vacancy cluster dissociation into smaller vacancy clusters.

The variation of $A^{\mathrm{B}}_{n\mathrm{v},\epsilon}$ with respect to n determines the dissociation probability [22]; while an n-vacancy cluster is thermally stable under a positive and rapidly increasing $A^{\mathrm{B}}_{n\mathrm{v},\epsilon}$ function, a negative and slowly increasing $A^{\mathrm{B}}_{n\mathrm{v},\epsilon}$ would result in a high dissociation probability of the n-vacancy cluster. Although the concentration of vacancy clusters is obtained under the equilibrium conditions, we believe that it could approximately represent the rate of dissociation at the non-equilibrium supersaturation conditions in which voids are formed [22].

With equations (5)–(7), we can evaluate the binding entropy $S^{\mathrm{B}}_{n\mathrm{v},\epsilon}$, and then the Helmholtz binding free energy of an n-vacancy cluster $A^{\mathrm{B}}_{n\mathrm{v},\epsilon}$ at a given temperature T. In figure 14, we present $A^{\mathrm{B}}_{n\mathrm{v},\epsilon}$ at $T = 300\,\mathrm{K}$ and $T = 900\,\mathrm{K}$ under the uniaxial and volumetric tensile strains.

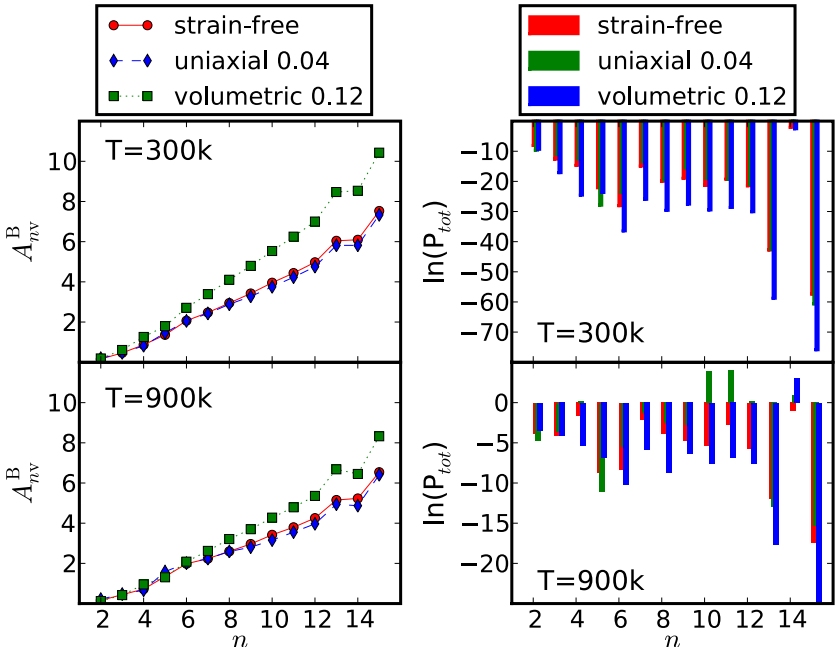

Figure 14. The Helmholtz binding free energy (eV) of n-vacancy clusters and the logarithm of the total dissociation probability $P_{\rm tot}$ at different temperatures for the strain-free (circle), uniaxial tensile strain (diamond) and volumetric tensile strain (square).

From the Helmholtz binding free energy, one can estimate the total dissociation probability $P_{\rm tot}(n)$ of an n-vacancy cluster, as plotted in the right panel of figure 14. The calculation reveals that the total dissociation probabilities of all n-vacancy clusters, except $n = 14$, are much less than 0.5 for both the strain-free and volumetric tensile strain conditions, which means they are thermodynamically stable. On the other hand, under the volumetric strain, the 14-vacancy cluster has more than 50% probability to dissociate into a 13-vacancy cluster and a monovacancy because $A^{\rm B}_{14{\rm v},\epsilon}$ is smaller than $A^{\rm B}_{13{\rm v},\epsilon}$. Under a uniaxial tensile strain, 10- and 11-vacancy clusters are not stable at $T = 900$ K; the 10- or 11-vacancy cluster has a high probability to dissociate into two 5-vacancy clusters or one 5- and one 6-vacancy clusters, respectively. In our previous study of Al, we find that at 300 K there is a critical size n^* ($n^* = 7$) below which the vacancy clusters are thermodynamically unstable with $P \geqslant 50\%$ [22]. For Cu, however, we find that the smaller vacancy clusters are actually thermodynamically stable with the exception of $n = 14$, which implies a greater n^*. At 900 K, in the presence of applied stress, the critical size n^* is reduced from 14 to 10. The dependence of the thermodynamic stability on applied stress is thus of importance for stress induced void formation.

4. Conclusion

We have examined the structure, mechanical and thermodynamic stability of the n-vacancy clusters where n goes from 2 to 21. We determine the most stable atomic structure of the vacancy clusters based on simple intuitive considerations and energetic calculations. More extensive (such as global search) and accurate (such as quantum mechanical) calculations are required to settle the issue with more confidence. This work should only be considered as a

preliminary effort. We find that the formation energy per vacancy decreases while the binding energy increases as a function of the cluster size n. We probe the mechanical stability of the vacancy clusters by applying the uniaxial and volumetric tensile strains. It is observed that yield stress and yield strain of the material are significantly reduced by the vacancy clusters. However, the presence of the vacancy cluster does not change the elastic behavior of the material before yielding. We find that the formation energy per vacancy decreases as a function of the uniaxial strain for all clusters, while the binding energy shows a more complicated behavior. For the volumetric deformations, the formation energy per vacancy increases first, then decreases as a function of the strain. The increase in the formation energy at smaller strains is due to the increased surface energy associated with the void. We determine the thermodynamic stability of the clusters by calculating the Helmholtz free binding energy and the resultant probability of dissociation. We find that most of the vacancy clusters under study are thermodynamically stable except the 14-vacancy cluster, which has a high probability of dissociating into a 13-vacancy cluster and a monovacancy. In addition, at 900 K the 10- and 11-vacancy clusters will dissociate into two 5-vacancy clusters or a 5- and a 6-vacancy clusters, respectively, under a uniaxial strain.

Acknowledgments

The work at California State University Northridge was supported by NSF PREM grant DMR-0611562 and DoE SciDAC grant DE-FC02-06ER25791.

References

[1] Fisher S B, White R J and Miller K M 1979 *Phil. Mag.* A **40** 239
[2] Zinkle S J, Seitzman L E and Wolfer W G 1987 *Phil. Mag.* A **55** 111
[3] Lu G and Kaxiras E 2005 *Phys. Rev. Lett.* **94** 155501
[4] Marian J, Knap J and Ortiz M 2004 *Phys. Rev. Lett.* **93** 165503
[5] Lu G and Kaxiras E 2002 *Phys. Rev. Lett.* **89** 105501
[6] Seeger A and Mehrer H 1970 *Vacancies and Interstitials in Metals* ed A Seeger *et al* (Amsterdam: North-Holland) p 1
[7] Neumann G 1989 *Defect Diffus. Forum* **43** 66
[8] Kraftmakher Y 1998 *Phys. Rep.* **299** 79
[9] Kittel C 1996 *Introduction to Solid State Physics* 7th edn (New York: Wiley)
[10] Li B Z, Sullivan T D, Lee T C and Badami D 2004 *Microelectron. Reliab.* **44** 365
[11] Wang R C J, Lee C C, Chen L D, Wu K and Chang-Liao K S 2006 *Microelectron. Reliab.* **46** 1673
[12] Wu Z Y, Yang Y T, Chai C C, Li Y J, Wang J Y, Liu J and Liu B 2008 *J. Microrel.* **48** 578
[13] Matsue T, Hanabusa T, Ikeuchi Y, Kusaka K and Sakata O 2006 *Vaccum* **80** 836
[14] Kolluri K, Gungor M R and Maroudas D 2008 *J. Appl. Phys.* **103** 123517
[15] Tszeng T C 2008 *J. Appl. Phys.* **103** 053509
[16] Uberuaga B P, Hoagland R G, Voter A F and Valone S M 2007 *Phys. Rev. Lett.* **99** 135501
[17] Rudd R E and Belak J F 2002 *Comput. Mater. Sci.* **24** 148
[18] Ahn D C, Sofronis P and Minich R 2006 *J. Mech. Phys. Solids* **54** 735
[19] Mukouda I and Shimomura Y 1999 *J. Nucl. Mater.* **271–272** 230
[20] Shimomura Y and Nishiguchi R 1997 *Radiat. Eff. Defects Solids* **141** 311
[21] Shimomura Y, Kiritani M and Mukouda I 2003 *Phil. Mag.* A **350** 238
[22] Zhang X and Lu G 2008 *Phys. Rev.* B **77** 174102
[23] Foiles S M, Baskes M I and Daw M S 1986 *Phys. Rev.* B **33** 7983
[24] Plimpton S J 1995 *J. Comput. Phys.* **117** 1
[25] Mishin Y, Sorensen M R and Voter A F 2001 *Phil. Mag.* A **81** 2591
[26] Carling K M, Wahnström G, Mattsson T R, Sandberg N and Grimvall G 2003 *Phys. Rev.* B **67** 054101
[27] Nordlund K and Averback R S 1998 *Phys. Rev. Lett.* **80** 4201
[28] Andersson D A and Simak S I 2004 *Phys. Rev.* B **70** 115108

[29] Perdew J P, Wang Y and Engel E 1991 *Phys. Rev. Lett.* **66** 508
[30] Carling K, Wahnström G, Mattsson T R, Mattsson A E, Sandberg N and Grimvall G 2000 *Phys. Rev. Lett.* **85** 3862
[31] Kelchner C L, Plimpton S J and Hamilton J C 1998 *Phys. Rev.* B **58** 11085
[32] Gavini V 2008 *Phys. Rev. Lett.* **101** 205503
[33] Vinet P, Rose J H, Ferrante J and Smith J R 1989 *J. Phys.: Condens. Matter* **1** 1941
[34] Grimvall G 1999 *Thermophysical Properties of Materials* (Amsterdam: Elsevier)
[35] Kelton K F 1991 *Solid State Physics* ed H Ehrenreich and D Turnbull (New York: Academic) vol 45 pp 75–177
[36] Kashchiev D 2000 *Nucleation: Basic Theory with Applications* (Oxford: Butterworth Heinemann)
[37] Soisson F and Martin G 2000 *Phys. Rev.* B **62** 203